Inorganic Chemistry
Article

Inorg. Chem. **2010**, *49*, 7331–7339 **7331**
DOI: 10.1021/ic100310w

Bistrimethylsilylamide Transition-Metal Complexes as Starting Reagents in the Synthesis of Ternary Cd−Mn−Se Cluster Complexes

Andreas Eichhöfer,*,† Oliver Hampe,†,‡ Sergei Lebedkin,† and Florian Weigend†,‡

†*Institut für Nanotechnologie,* ‡*Institut für Physikalische Chemie, Karlsruhe Institut für Technologie* (*KIT*), *Postfach 3640 76021 Karlsruhe, Germany*

Received February 14, 2010

The use of bis-trimethylsilylamide transition-metal complexes soluble in organic solvents offers new perspectives for the synthesis of metal chalcogenide cluster molecules, especially for multicomponent clusters. This is illustrated by the synthesis of the mixed cadmium−manganese chalcogenide clusters $[Cd_4Mn_6Se_4(SePh)_{12}(P^nPr_3)_4]$ and $[Cd_4Mn_4S(SePh)_{14}(P^nPr_3)_2]$ as reported here. These cluster molecules display interesting properties, such as a photoluminescence in the red to near-infrared spectral region, which is particularly bright at temperatures below ∼100 K, and an antiferromagnetic coupling between the manganese(II) ions. Electrospray Fourier transform ion cyclotron resonance mass spectra from the chemically charged clusters in solution show several ionic cluster species which indicate a fast Cd/Mn exchange in solution. Furthermore, single crystal X-ray analysis and magnetic measurements supported by density functional theory calculations suggest a cocrystallization of structural isomers of the ideal cluster composition $[Cd_4Mn_4S(SePh)_{14}(P^nPr_3)_2]$ as well as of species with the general formula $[Cd_{4+x}Mn_{4-x}S(SePh)_{14}(P^nPr_3)_2]$ ($x < 0$ Mn enrichment; $x > 0$ Cd enrichment) without a significant decrease in the stability. Thermal cleavage of $[Cd_4Mn_6Se_4(SePh)_{12}(P^nPr_3)_4]$ results, in agreement with the CdSe/MnSe phase diagram, in the formation of a mixture of a hexagonal phase $Cd_{1-x}Mn_xSe$ ($x \approx 0.5$) and a cubic phase $Mn_{1-x}Cd_xSe$ ($x < 0.05$).

Introduction

The synthesis of ternary cluster molecules and nanoparticles has recently attracted a considerable interest.[1] Ternary compounds offer, in comparison to binary ones, a broader spectrum of tunable properties and are viable candidates for a number of technical applications. For instance, $CuInSe_2$ is one of the most promising materials for the thin-film solar cell technology. Of importance are not only a further development of synthetic methods and a structural characterization of cluster molecules and nanoparticles of ternary compounds but also an investigation of correlations between their properties and structure, size, and composition. A high sensitivity of the electronic properties to the structure and composition is illustrated, for instance, by photoluminescence (PL) data. Thus, Corrigan et al. have observed a bright room temperature PL for the ternary 12-12′-16 cluster (12 = Zn; 12′ = Cd; 16 = Se), $[(N,N'\text{-tmeda})_5Zn_5Cd_{11}Se_{13}(SePh)_6(thf)_2]$,[2] whereas the binary cadmium or zinc selenide clusters showed only a weak emission at temperatures below 50 K.[3,4] A strong infrared PL has been found by Brennan and co-workers to occur in heterometallic chalcogenido cluster molecules $[(py)_8Ln_4M_2Se_6(SePh)_4]$ (Ln = Er; M = Cd, Hg)[5] and $[(py)_{18}Nd_{12}O_6Se_4(Se_2)_4(SePh)_4(Se_2Ph)_2Hg_2(SePh)_4][(Hg(SePh)_3]_2$.[6]

Manganese has been actively used as a dopant for 12-16 semiconductor films and nanocrystals, usually referred to as dilute magnetic semiconductors (DMS).[7−9] The studies of this important class of materials have motivated the synthesis of manganese-doped 12-16 semiconductor nanoparticles as well as the investigation of their magnetic and optical properties.[10] Along with the experimental efforts, there is also an interest from a theoretical sight to understand diffusion barriers and 'self-purification' processes of the manganese 'impurity' in these systems.[11]

*Corresponding author. Telephone: + 7247-82-6371. Fax: + 7247-82-6368. E-mail: andreas.eichhoefer@kit.edu.

(1) Dehnen, S.; Melullis, M. *Coord. Chem. Rev.* **2007**, *251*, 1259–1280.
(2) DeGroot, M. W.; Taylor, N. J.; Corrigan, J. F. *J. Am. Chem. Soc.* **2003**, *125*(4), 864–865.
(3) Soloviev, V.; Eichhöfer, A.; Fenske, D.; Banin, U. *J. Am. Chem. Soc.* **2000**, *122*, 2673–2674.
(4) Soloviev, V.; Eichhöfer, A.; Fenske, D.; Banin, U. *J. Am. Chem. Soc.* **2001**, *123*, 2354–2364.
(5) Kornienko, A.; Banerjee, S.; Kumar, G. A.; Riman, R. E.; Emge, T. J.; Brennan, J. G. *J. Am. Chem. Soc.* **2005**, *127*, 14008–14014.
(6) Banerjee, S.; Kumar, G. A.; Riman, R. E.; Emge, T. J.; Brennan, J. G. *J. Am. Chem. Soc.* **2007**, *129*, 5926–5932.
(7) Furdyna, J. K. *J. Appl. Phys.* **1988**, *64*, R29–R64.
(8) Norris, D. J.; Yao, N.; Charnock, F. T.; Kennedy, T. A. *Nano Lett.* **2001**, *1*, 3–7.
(9) Mikulec, F. V.; Kuno, M.; Bennati, M.; Hall, D. A.; Griffin, V.; Bawendi, M. G. *J. Am. Chem. Soc.* **2000**, *122*, 2532–2540.
(10) for a recent overview, see: Beaulac, R.; Archer, P. I.; Ochsenbein, T.; Gamelin, D. R. *Adv. Funct. Mat.* **2008**, *18*, 3873–3891.

Published on Web 07/21/2010

Scheme 1. Mixed Cadmium Manganese Selenide/Selenolate Cluster Complex $[Cd_4Mn_6Se_4(SePh)_{12}(P^nPr_3)_4]$ (1)

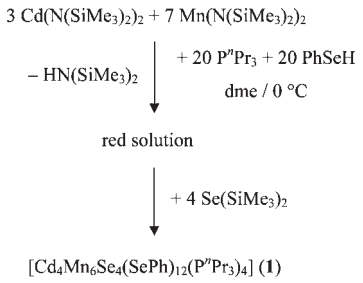

Scheme 2. Mixed Cadmium Manganese Sulfide/Selenolate Cluster Complex $[Cd_4Mn_4S(SePh)_{14}(P^nPr_3)_2]$ (2)

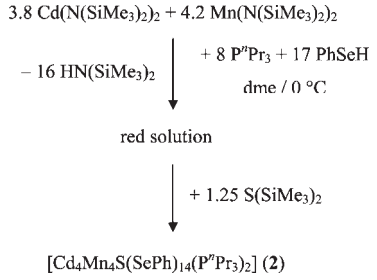

Cluster complexes represent a 'molecular limit' of nanoparticle systems.[3,4] Here, we report on the synthesis of two cadmium manganese selenolate cluster complexes by reaction of bis-trimethylsilylamide transition-metal complexes with HSePh and $E(SiMe_3)_2$ (E = S, Se) along with their structural and mass spectrometric characterization as well as an investigation of their magnetic, thermal, and optical properties. Silylchalcogenides have been first used in the synthesis of chalcogenido materials by Steigerwald and co-workers[12] and subsequently established in the synthesis of metal chalcogenide cluster molecules by Fenske et al.[13,14]

Results and Discussion

Synthesis and Structure. Reaction of a 3:7 mixture of $Cd(N(SiMe_3)_2)_2$ and $Mn(N(SiMe_3)_2)_2$ with PhSeH and subsequent addition of $Se(SiMe_3)_2$ in the presence of P^nPr_3 in dme yielded red crystals of the mixed cadmium manganese selenide/selenolate cluster complex $[Cd_4Mn_6Se_4(SePh)_{12}(P^nPr_3)_4]$ (**1**) in accordance to Scheme 1.

However, when reacting a 1:1 mixture of the same metal precursors with PhSeH and adding $S(SiMe_3)_2$ one obtains – again in the presence of P^nPr_3 in dme – light red crystals of the mixed cadmium manganese sulfide/selenolate cluster complex $[Cd_4Mn_4S(SePh)_{14}(P^nPr_3)_2]$ (**2**) according to Scheme 2.

Compound **1** crystallizes in the cubic space group *F*-43*c* with two independent molecules in the asymmetric unit (Table 1). Because the structures of the two clusters including bond lengths and angles are quite similar, only one is mapped and discussed in the following. The tetrahedrally shaped cluster core (Figure 1) is composed of four fused distorted $\{CdMn_3Se_6\}$ adamantoid cages with Cd(1) residing on a three-fold and Mn(1) on a two-fold axis. In this way, all six manganese atoms (Mn(1) and symmetry equivalent positions) and four μ_3-Se^{2-} ligands (Se(2) and symmetry equivalent positions) build a central adamantoid cage $[Mn_6Se_4]^{4+}$, which is face capped by four $[(\mu_2\text{-}SePh)_3Cd(P^nPr_3)]^-$ (Cd(1), Se(1), P(1), and symmetry

Table 1. Crystallographic Data for $[Cd_4Mn_6Se_4(SePh)_{12}(P^nPr_3)_4]$ (**1**) and $[Cd_4Mn_4S(SePh)_{14}(P^nPr_3)_2]$ (**2**)

	1	**2** · 3dme
fw (g/mol)	3608.71	3476.07
crystal system	cubic	triclinic
space group	*F*-43*c*	*P*-1
a (pm)	3729.5(4)	1452.0(3)
b		1785.7(4)
c		2678.7(5)
α		95.86(3)
β		91.76(3)
γ (°)		112.93(3)
V (10^9pm^3)	51 876(10)	6344(2)
Z	16	2
T (K)	190	180
d_c (g cm^{-3})	1.848	1.820
μ (mm^{-1})	5.785	5.148
F[000]	27 808	3374
$2\theta_{max}$ (°)	49	50
meas reflns	33 776	56 155
unique reflns	3632	22 545
R_{int}	0.0884	0.0552
reflns with $I > 2\sigma(I)$	3173	17 883
refined params	209	1318
$R1(I > 2\sigma(I))^a$	0.0442	0.0493
$wR2$(all data)^b	0.1347	0.1288
abs struct parameter	0.039(19)	

$^a R1 = \sum||F_o| - |F_c||/\sum|F_o|$. $^b wR2 = \{\sum[w(F_o^2 - F_c^2)^2]/\sum[w(F_o^2)^2]\}^{1/2}$.

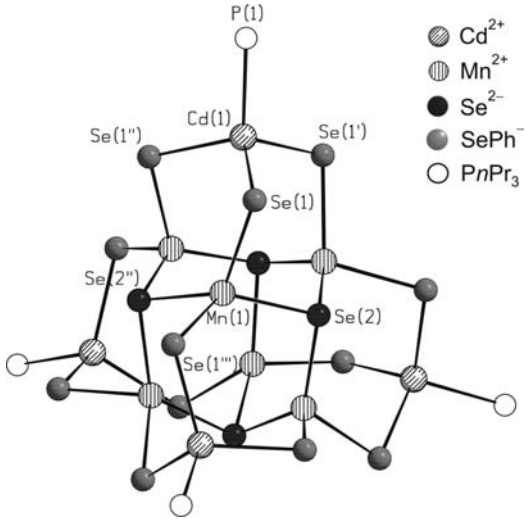

Figure 1. Molecular structure of the cluster $[Cd_4Mn_6Se_4(SePh)_{12}(P^nPr_3)_4]$ (**1**). C and H atoms are omitted for clarity. Selected bond lengths [pm] and angles [°]: Cd(1)–P(1), 255.8(5); Cd(1)–Se(1), 264.00(11); Mn(1)–Se(2), 251.96(13); Mn(1)–Se(1), 262.23(14); P(1)–Cd(1)–Se(1), 109.24(3); $Se(1)^I$–Cd(1)–Se(1), 109.71(3); $Se(2)–Mn(1)–Se(2)^{III}$, 127.31(11); $Se(2)–Mn(1)–Se(1)^{III}$, 121.79(3); Se(2)–Mn(1)–Se(1), 90.34(4); $Se(1)^{III}$–Mn(1)–Se(1), 106.24(7). Symmetry transformation for the generation of equivalent atoms: $^I -z + 1, -x + 1/2, y + 1/2$; $^{II} -y + 1/2, z - 1/2, -x + 1$; $^{III} x, -y + 1, -z + 2$.

(11) see e.g.: Chan, T.-L.; Zayak, A. T.; Dalpin, G. M.; Chelikowsky, J. R. *Phys. Rev. Lett.* **2009** *102*, 025901 and references therein.
(12) Stuczynski, S. M.; Brennan, J. G.; Steigerwald, M. L. *Inorg. Chem.* **1989**, *28*, 4431–4432.
(13) Dehnen, S.; Eichhöfer, A.; Fenske, D. *Eur. J. Inorg. Chem.* **2002**, 279–317.
(14) Corrigan, J. F.; Fuhr, O.; Fenske, D. *Adv. Mater.* **2009**, *21*, 1867–1871.

equivalent positions) units through μ_2-SePh$^-$ ligands. All cadmium and manganese atoms display a distorted tetrahedral coordination environment [bond angles: Se−Mn−Se, 90.32(4)−127.32(12)°; Se−Cd−Se, 109.67(4)°; P−Cd−Se, 109.28(4)°]. Mn(1)−μ_3-Se(2) bond distances (252.64(14) pm) are found to be shorter than the corresponding Mn(1)−μ_2-Se(1) bond lengths (262.46(14) pm) and are comparable to values reported for related pure manganese selenolato/selenide cluster molecules $[Mn_{32}Se_{14}(SePh)_{36}(P^nPr_3)_4]$ and $[Mn_8Se(SePh)_{16}]^{2-}$.[15] The Cd(1)−μ_2-Se(1) (264.16(11) pm) and Cd(1)−P(1) (258.2(5) pm) bond lengths are similar to those observed in related $[Cd_{10}Se_4(SePh)_{12}(P^nPr_3)_4]$.[4] The so-formed tetrahedral cluster cage is isostructural to known binary and ternary cluster molecules like $[Cd_{10}(SCH_2CH_2OH)_{16}]^{4+}$,[16] $[M_{10}E_4(SPh)_{16}]^{4-}$ (M = Zn, Cd, E = S, Se),[17,18] and $[M_{10}E_4(E'Ph)_{12}(PR_3)_4]$ (M = Zn, Cd, Hg; E, E′ = S, Se, Te; R = organic group).[19−25] As a result of the X-ray structure analysis, each independent cluster molecule in the crystal structure comprises only two metal atom positions which are nonequivalent in symmetry, suggesting the overall formula $[Cd_4Mn_6Se_4(SePh)_{12}(P^nPr_3)_4]$. In order to support this stoichiometry, the metal composition of **1** in the crystal was measured by inductively coupled plasma atomic emission spectroscopy (ICP-AES) to be 4:6 Cd:Mn.

The calculated (190 K) and measured powder patterns (293 K) of **1** show a very good agreement taking into account the temperature difference, and there is no indication for the strongest [101] reflection (2θ = 5.564°) of the analogous pure cadmium selenide cluster $[Cd_{10}Se_4(SePh)_{12}(P^nPr_3)_4]$[4] (Figure S1, Supporting Information). However, the single crystal X-ray data refine slightly better [$wR2$ (all data) before: 0.1402; after: 0.1347] when the cadmium and manganese atoms were allowed to slightly mix in such a way that 10% of the Cd atoms (0.4 Cd) reside on the manganese positions and vice versa. Note that the ionic radii for the four-fold-coordinated metal ions are different ($r_{Mn(II)}$ (hs): 80; $r_{Cd(II)}$: 92 pm). A 50% mixing of different atoms on the same atom position can originate for example from cocrystallization of two different Cd_4Mn_6 cluster molecules with intra-exchanged positions. It is on the other hand also possible that two different sorts of clusters with inter-exchanged atoms, e.g., Cd_3Mn_7 and Cd_5Mn_5, crystallize in one crystal. The situation is, therefore, roughly comparable to a series of recently reported ternary nanoclusters $[Zn_xCd_{10-x}E_4(EPh)_{12}(P^nPr_3)_4]$ (E = Se, Te, x = 1.8, 2.6), $[Zn_3Hg_7Se_4(SePh)_{12}(P^nPr_3)_4]$ and $[Cd_{3.7}Hg_{6.3}Se_4(SePh)_{12}(P^nPr_3)_4]$,[24,25] which all comprise the same structural $M_{10}Se_4(SePh)_{12}(P^nPr_3)_4$ cluster motif. For those structures it was not possible to fully resolve the positions of the different metal atoms from the crystallographic data, which suggests an intimate mixing of the metal atoms over all 10 metal atom positions (for further details see following discussions).

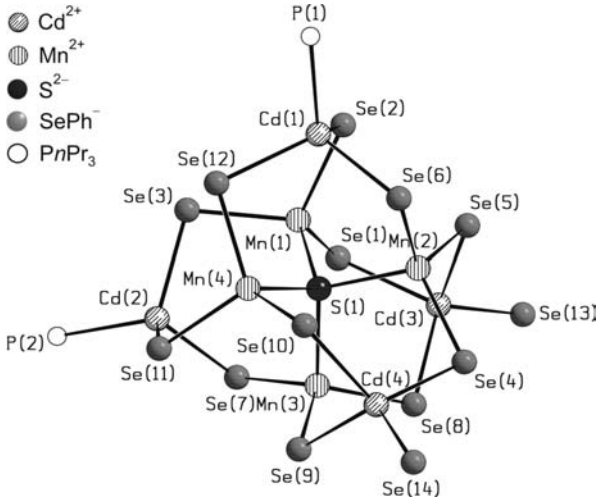

Figure 2. Molecular structure of the cluster $[Cd_4Mn_4S(SePh)_{14}(P^nPr_3)_2]$ (**2**). C and H atoms are omitted for clarity. Selected bond lengths [pm]: Cd(1)−P(1), 256.89(19); Cd(2)−P(2), 256.8(2); Cd(1)−Se(6), 262.81(13); Cd(1)−Se(2), 264.66(11); Cd(1)−Se(12), 265.81(10); Cd(2)−Se(7), 262.98(9); Cd(2)−Se(3), 264.79(10); Cd(2)−Se(11), 265.78(13); Cd(3)−Se(13), 251.67(11); Cd(3)−Se(8), 265.70(12); Cd(3)−Se(5), 268.19(11); Cd(3)−Se(1), 269.83(13); Cd(4)−Se(14), 253.86(15); Cd(4)−Se(4), 265.61(11); Cd(4)−Se(9), 268.20(13); Cd(4)−Se(10), 268.48(10); Mn(1)−S(1), 243.2(2); Mn(1)−Se(1), 256.31(12); Mn(1)−Se(3), 257.80(13); Mn(1)−Se(2), 258.65(12); Mn(2)−S(1), 244.53(19); Mn(2)−Se(5), 254.41(13); Mn(2)−Se(4), 254.63(15); Mn(2)−Se(6), 257.49(12); Mn(3)−S(1), 243.68(17); Mn(3)−Se(8), 254.09(12); Mn(3)−Se(9), 255.81(15); Mn(3)−Se(7), 258.27(15); Mn(4)−S(1), 244.33(17); Mn(4)−Se(10), 254.95(16); Mn(4)−Se(12), 257.32(13); Mn(4)−Se(11), 258.28(13).

The tetrahedral cluster **2** crystallizes in the triclinic space group *P*-1, and its molecular structure is shown in Figure 2. The central sulfur atom S(1) is tetrahedrally surrounded by four inner manganese atoms Mn(1)−Mn(4) (Figure 2). Each of these four inner manganese atoms is bound through three μ_2-PhSe$^-$ ligands Se(1)−Se(12) to one of the four outer-shell cadmium atoms Cd(1)−Cd(4), which also form a tetrahedron. In addition, two of the four outer cadmium atoms Cd(3) and Cd(4) are bound to a terminal PhSe$^-$ ligand (Se(13), Se(14)), whereas Cd(2) and Cd(1) are bound to a terminal P^nPr_3 ligand (P(1), P(2)). All of the eight transition-metal atoms adopt a distorted tetrahedral coordination sphere [S−Mn−Se, 100.90(5)−110.09(5)°; Se−Mn−Se, 107.67(4)−116.06(5)°; Se−Cd−Se, 98.49(4)−120.08(4)°; Se−Cd−P, 105.18(5)−112.63(6)°]. The ranges of M−μ_2-SePh bond lengths [M = Cd, Mn; (Se(8)−Mn(3), 254.09(12) pm, to Se(2)−Mn(1), 258.65(12) pm; Se(7)−Cd(2), 262.98(9) pm, to Se(1)−Cd(3), 269.83(13) pm] are similar to those found in $[Cd_8Se(SePh)_{12}Cl_4]^{2-}$[26] and $[Mn_8Se(SePh)_{16}]^{2-}$,[15] while Cd−μ_1-SePh (251.67(11)−253.86(15) pm), Cd−P (256.89(19) and

(15) Eichhöfer, A.; Wood, P. T.; Viswannath, R. N.; Mole, R. N. *J. Chem. Soc. Chem. Commun.* **2008**, 1596–1598.
(16) Strickler, P. *J. Chem. Soc. D* **1969**, 655b–656.
(17) Choy, A.; Craig, D.; Dance, I. G.; Scudder, M. L. *J. Chem. Soc. Chem. Commun.* **1982**, 1246–1247.
(18) Dance, I. G.; Choy, A.; Scudder, M. L. *J. Am. Chem. Soc.* **1984**, *106*, 6285–6295.
(19) Behrens, S.; Bettenhausen, M.; Eichhöfer, A.; Fenske, D. *Angew. Chem.* **1997**, *109*, 2874–2876. Behrens, S.; Bettenhausen, M.; Eichhöfer, A.; Fenske, D. *Angew. Chem., Int. Ed. Engl.* **1997**, *24*, 2797-2799.
(20) Eichhöfer, A.; Fenske, D.; Pfistner, H.; Wunder, M. *Z. Anorg. Allg. Chem.* **1998**, *624*, 1909–1914.
(21) Eichhöfer, A.; Aharoni, A.; Banin, U. *Z. Anorg. Allg. Chem.* **2002**, *628*, 2415–2421.
(22) Eichhöfer, A.; Tröster, E. *Eur. J. Inorg. Chem.* **2002**, 2253–2256.
(23) Eichhöfer, A.; Deglmann, P. *Eur. J. Inorg. Chem.* **2004**, 349–355.
(24) De Groot, M. W.; Corrigan, J. F. *Angew. Chem., Int. Ed.* **2004**, *43*, 5355–5357.
(25) DeGroot, M. W.; Taylor, N. J.; Corrigan, J. F. *Inorg. Chem.* **2005**, *44*, 5447–5458.
(26) Eichhöfer, A.; Hampe, O.; Blom, M. *Eur. J. Inorg. Chem.* **2003**, 1307–1314.

256.8(2) pm), and Mn−S (243.2−244.53(2) pm) compare rather with those found in $[Cd_{17}Se_4(SePh)_{24}]^{2-}$,[27] **1**, $[Cd_{10}Se_4(SePh)_{12}(P^nPr_3)_4]$,[4] and $[Cu_4Mn_4S(S^iC_3H_7)_{12}]^{2-}$,[28] respectively. Similar to **1**, refinement of the model for **2** with a slightly mixed occupancy of the cadmium and manganese positions results in better *R* values [*wR*2 (all data) before: 0.1498; after: 0.1284]. Interestingly, the mixing is only indicated for the cadmium atoms Cd(3) and Cd(4) (by 20%) which are coordinated to the two terminal $SePh^-$ groups (Se(13), Se(14)), while it is equally (10%) distributed over all four manganese positions. The suggested overall Cd−Mn ratio, however, is 4:4 (Cd:Mn) which was also determined by ICP-AES. Structurally related $[M_8E(ER)_{16}]^{2-}$ (M = Zn, Cd; E = S, Se, Te; R = organic group) cluster cages are a well-known motif in the cluster chemistry of group 12 metal chalcogenides.[26,29] A related linear trinuclear thiolato complex which incorporates cadmium and manganese atoms, namely $[(MnL_2)_2Cd]^{2+}$ (L = $^-S-(C_2H_4)-NH-(C_3H_6)-NH_2$), has been synthesized before.[30]

Interestingly, we found that both reaction solutions (see Schemes 1 and 2) with the formally correct Cd:Mn ratio of 4:6 or 4:4, respectively, yield crystals similar to **1** and **2**. However, ICP-AES analysis of the resulting crystalline powders and refinement of the single crystal X-ray diffraction data suggest the average formulas $[Cd_{4.6}Mn_{5.4}Se_4(SePh)_{12}(P^nPr_3)_4]$ and $[Cd_{4.2}Mn_{3.8}S(SePh)_{14}(P^nPr_3)_2]$ having a higher cadmium content as compared to **1** and **2**. This indicates that it should be possible to adjust the overall cluster composition (narrow spectrum of different individuals) by adjusting the reaction stoichiometry of the metal salts. Finally very low concentrations of the manganese precursor might thus lead to a magnetic doping of, for example, $[Cd_{10}Se_4(SePh)_{12}(P^nPr_3)_4]$ cluster molecules. We are currently investigating this issue in more detail.

Mass Spectrometry. Although crystallization is usually an excellent purification process, it might be conceivable as already mentioned before, that, for example, in the case of compound **1** molecules like $[Cd_{4+x}Mn_{6-x}Se_4(SePh)_{12}(P^nPr_3)_4]$ ($x < 0$ Mn enrichment; $x > 0$ Cd enrichment) cocrystallize giving the overall ideal formula $[Cd_4Mn_6Se_4(SePh)_{12}(P^nPr_3)_4]$. We, therefore, intended to investigate the Cd:Mn ratio of the compounds **1** and **2** by mass spectrometeric techniques, which have been proven to be very useful for elucidation of atomic compositions of large inorganic cluster molecules, such as $[Ag_{26}In_{18}S_{36}Cl_6(dppm)_{10}(thf)_4]^{2+}$[31] or $[Au_{19}(As^nPr)_8(dppe)_6]^{3+}$.[32] For neutral cadmium selenide cluster molecules, a chemical ligand exchange with $SePh^-$ replacing phosphane groups has been recently successfully applied in our laboratory to generate multianionic species in the gas phase.[27,33] In an analogous fashion, we now reacted **1** and **2** with one mole equivalent of NaSePh and obtained pale rose-red solutions which were directly injected into the electrospray source of the mass spectrometer. However, the mass spectrometric probes of **1** (Figure S2, Supporting Information) indicated that the cluster is severely restructuring in solution leading among others to the formation of a mixed eight-metal atom species, namely $[Cd_{8-x}Mn_xSe(SePh)_{16}]^{2-}$.

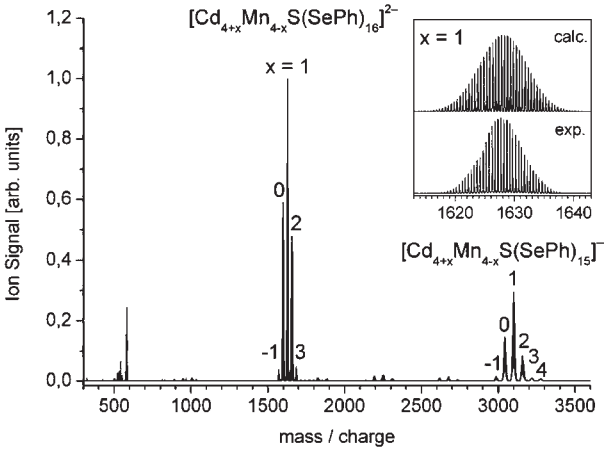

Figure 3. Negative-ion electrospray FT-ICR mass spectrum from a solution of $[Cd_4Mn_4S(SePh)_{14}(P^nPr_3)_2]$ (**2**) and NaSePh in thf. Single- and double-charged molecular anions are labeled according to their relative metal content. The inset shows a comparison of isotopomere-resolved peaks from experiment and simulation.

The FT-ICR mass spectra of solutions of **2** in negative-ion mode are shown in Figure 3 and are dominated by two groups of peaks of singly and doubly charged anions in the *m*/*z* range of 2970−3300 and 1560−1700, respectively. In contrast to the findings for **1**, the isotopomer-resolved peaks for **2** allow us to identify them clearly as molecular species with the general composition $[Cd_{4+x}Mn_{4-x}S(SePh)_{15}]^-$ and $[Cd_{4+x}Mn_{4-x}S(SePh)_{16}]^{2-}$. This indicates that in solution the clusters indeed loose the P^nPr_3 groups, and one or two $SePh^-$ ions are added without significant disintegration. Second, we observe that the cadmium and manganese metal ions can indeed exchange in solution. The distribution of anionic molecular peaks in the mass spectrum is centered around $x = 1$ (see Figure 3) pointing toward an enrichment of cadmium with regard to the composition of **2**. Such a metal exchange behavior has been reported before for cadmium/zinc thiophenolate clusters.[34]

Quantum Chemical Calculations. From single crystal X-ray data of both compounds **1** and **2**, the spatial distribution of cadmium and manganese ions shown in Figures 1 and 2 are the most probable ones, $\mathbf{1}_{best}$ and $\mathbf{2}_{best}$, but as the *R* values improve for slightly mixed occupancies of cadmium and manganese positions, it appears plausible that also other distributions could be realized. This is possible only if they are of similar stability as $\mathbf{1}_{best}$ or $\mathbf{2}_{best}$, respectively. In the following we apply methods of density functional theory (DFT) using the program

(27) Eichhöfer, A.; Hampe, O. *J. Cluster Sci.* **2007**, *18*, 494–504.
(28) Stephan, H.-O.; Kanatzidis, M. G.; Henkel, G. *Angew. Chem., Int. Ed.* **1996**, 2135–2137.
(29) Lee, G. S. H.; Fisher, K. J.; Craig, D. C.; Scudder, M. L.; Dance, I. G. *J. Am. Chem. Soc.* **1990**, *112*, 6435–6437.
(30) Mikuriya, M.; Tsutsumi, H.; Nukada, R.; Handa, M.; Sayama, Y. *Bull. Chem. Soc. Jpn.* **1996**, *69*, 3489–3498.
(31) Ahlrichs, R.; Eichhöfer, A.; Fenske, D.; Hampe, O.; Kappes, M.; Nava, P.; Olkowska-Oetzel, J. *Angew. Chem., Int. Ed.* **2004**, *43*, 3823–3827.
(32) Sevillano, P.; Fuhr, O.; Kattannek, M.; Nava, P.; Hampe, O.; Lebedkin, S.; Ahlrichs, R.; Fenske, D.; Kappes, M. M. *Angew. Chem., Int. Ed.* **2006**, *45*, 3702–3708.
(33) Eichhöfer, A.; Hampe, O. *Chem. Phys. Lett.* **2005**, *407*, 186–191.
(34) Løver, T.; Henderson, W.; Bowmaker, G. A.; Seakins, J. M.; Cooney, R. P. *Inorg. Chem.* **1997**, *36*, 3711–3723.

system TURBOMOLE[35] to investigate this for compound **2** with all phenyl and *n*-propyl groups exchanged by $-CH_3$. Due to the similarity of the two compounds, the results for **1** are expected to be similar. For a complete treatment, one would have to consider all 70 possibilities to distribute four manganese and four cadmium ions on eight atom sites and for each of these possibilities the high-spin state and six low-spin states. But for our purposes, it is sufficient to show that at least some isomers are energetically close to $\mathbf{2}_{best}$.

First $\mathbf{2}_{best}$ was treated assuming C_2 symmetry, i.e., optimizations of the structure parameters of the high-spin state (involving four spin-up manganese(II) ions) as well as of the three symmetry-distinct low-spin broken-symmetry states (involving two spin-up and two spin-down manganese(II) ions) were carried out using the BP86 functional[36,37] and def2-SV(P)[38] basis sets. Subsequently the energies were recalculated without further structure optimization using the B3-LYP functional[39] and larger def2-TZVP basis sets;[38] this choice is computationally much more demanding, but is known to give more reliable results for the energies of the low-spin states, whereas structure parameters are similar for both cases.[40] The three low-spin states were found to be of very similar energy (within 1 kJ/mol), the high-spin state is higher in energy by ca. 10 kJ/mol. Next, numerous other distributions of Cd and Mn were treated; we restricted our considerations to cases where only one or two atoms change their sites. For all cases at first, the high-spin state was treated, then for all spin-orientations the sequence of energy gains from antiferromagnetic interactions was estimated by summing for every possible orientation r^{-4} for all distances r between manganese ions of opposite spin (assuming dipole−dipole interactions). The most promising low-spin state found in this way was treated as described above. The results are shown in Figure 4 as well as the mean absolute deviations of all metal-chalcogen distances compared to the X-ray structure, $\varnothing_{\Delta d}$. The data reveal the following trends. The energetically lowest-lying isomers also show the best agreement with the experimental structure parameters; the observed overestimation, $\varnothing_{\Delta d} \approx 3$ pm, is typical for the BP-functional in these cases;[40] furthermore, these values are very similar for the high- and low-spin states. Isomers that are only ca. 7−10 kJ/mol higher in energy than $\mathbf{2}_{best}$ are found, cadmium ions with terminal $SePh^-$ ligands (atom positions 3 and 4) are involved in the Mn−Cd swapping. This energy difference is small enough to allow the formation of those isomers, in particular, if the errors of the method are regarded. For isomer B, where only one position is exchanged, the difference to the experimental structure parameters is somewhat larger, $\varnothing_{\Delta d} = 5.2$ pm. Thus, regarding both energy and structure parameters, this

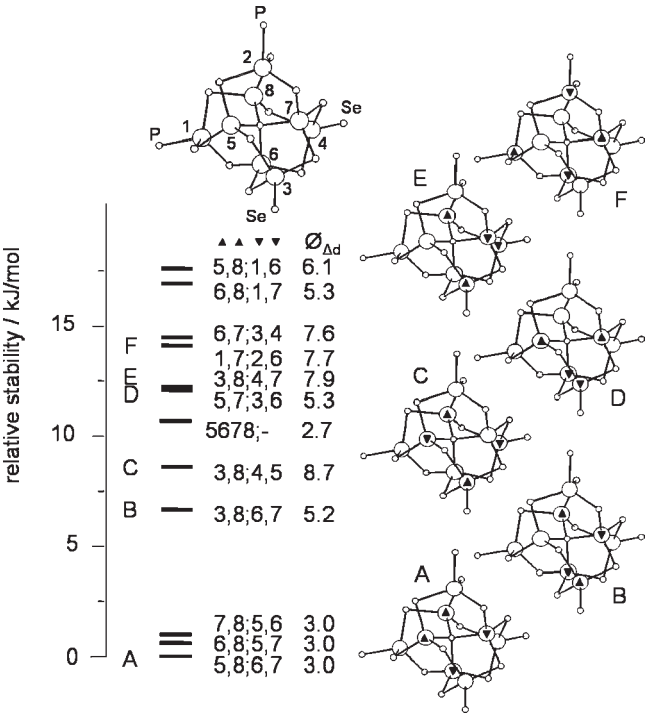

Figure 4. Calculated relative stabilities for selected isomers of $[Cd_4Mn_4S(SeMe)_{14}(PMe_3)_2]$ (Me = CH_3) within the broken symmetry approach. The numbers to the right of the levels indicate the positions of the manganese atoms. The numbers to the left of the semicolon denote manganese atoms with five unpaired spin-up electrons, those to the right of the semicolon denote that with five spin-down electrons. For convenience, selected isomers (A−F) additionally are shown at the left-hand side. The numbers in the column "$\varnothing_{\Delta d}$" are the mean absolute deviations (in pm) of the calculated metal-chalcogene distances compared to the X-ray data for the respective isomers.

isomer is quite close to 2_{best}. For isomer C, where two positions are exchanged, $\varnothing_{\Delta d}$ amounts to 8.7 pm, which is nontypically high; this isomer probably can be ruled out. Involving cadmium atoms ligated by phosphine ligands (atom positions 1 and 2) seems to be slightly less favorable; the energetically lowest of these isomers is ca. 14 kJ/mol higher in energy than $\mathbf{2}_{best}$; $\varnothing_{\Delta d}$ here typically amounts to ca. 7−8 pm, even if only one atom is exchanged. Swaps of this type are less probable. The calculations indicate that the exchange of one Mn−Cd pair, in particular with the Cd atom not being ligated by phosphine, is possible. One might also consider the possibility, that the ratio Cd:Mn = 4:4 in the solid-state results from appropriate mixing of individual molecules with other stoichiometries, e.g., Cd_5Mn_3 plus Cd_3Mn_5 (the ligands are unchanged, they are not explicitly listed for simplicity). This possibility was estimated by the energy of the reaction $2Cd_4Mn_4 \rightarrow Cd_5Mn_3 + Cd_3Mn_5$.

For the left-hand side, $\mathbf{2}_{best}$ was chosen, and for the right-hand side, the Mn atoms occupy positions 6−8 in Mn_3Cd_5 and additionally position 4 and 3 in Mn_5Cd_3. This distribution was chosen as the Mn/Cd exchange seems to be most easily for positions 4 and 3 (see above); for all cases, the high-spin states were taken. With the energies obtained at B3-LYP/def2-TZVP level using B-P/def2-SV(P) geometry (see above), the disproportion energy amounts to only 0.2 kJ/mol, which is negligibly small. Comparison of distances with experimental data supports

(35) *TURBOMOLE*, v 6.0; TURBOMOLE GmbH: Karlsruhe, Germany, 2009; http://www.turbomole.de.
(36) Becke, A. D. *J. Chem. Phys.* **1993**, *98*, 5648–5652.
(37) Perdew, J. P. *Phys. Rev. B: Condens. Matter Mater. Phys.* **1986**, *33*, 8822–8824.
(38) Weigend, F.; Ahlrichs, R. *Phys. Chem. Chem. Phys.* **2005**, *7*, 3297–3305.
(39) Lee, C.; Yang, W.; Parr, R. G. *Phys. Rev. B: Condens. Matter Mater. Phys.* **1988**, *37*, 785–789.
(40) Hänisch, C. K. F. v.; Weigend, F.; Clérac, R. *Inorg. Chem.* **2008**, *47*, 1460–1464.

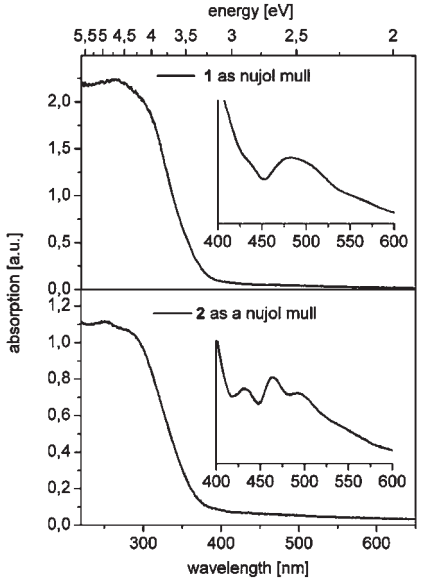

Figure 5. UV−vis spectra of $[Cd_4Mn_6Se_4(SePh)_{12}(P^nPr_3)_4]$ (**1**) and $[Cd_4Mn_4S(SePh)_{14}(P^nPr_3)_2]$ (**2**) as a mull in nujol. The insets display a section of the UV−vis spectra from concentrated nujol mulls of **1** and **2**.

this possibility; for Mn_3Cd_5, $\varnothing_{\Delta d}$ amounts to 4.9 pm, and for Mn_5Cd_3, only to 2.7 pm. Also the Cd_2Mn_6 species (Cd at the positions binding to the $SePh^-$ ligands) appear to be accessible; the reaction energy of $3Cd_4Mn_4 \rightarrow Cd_2Mn_6 + 2Cd_5Mn_3$ (calculated as above) is 0.9 kJ/mol, and $\varnothing_{\Delta d}$ amounts to 2.8 pm for Cd_2Mn_6.

The calculations, therefore, suggest that in the solid-state structures of **1** and **2**, a kinetically controlled exchange on the cadmium and manganese sites as well as the occurrence of Cd_3Mn_5 or Cd_5Mn_3 or Cd_2Mn_6 species is possible.

Optical Properties. UV−vis absorption spectra of crystals of **1** and **2** measured in either the solid state (as nujol mull) (Figure 5) or as solutions in thf (Figure S3, Supporting Information) display similar features. Also, the spectra are quite similar to those of related pure manganese chalcogenide clusters $[Mn_8Se(SePh)_{16}]^{2-}$ and $[Mn_{32}Se_{14}(SePh)_{36}(P^nPr_3)_4]$.[15] The spectra are dominated by a broad absorption feature in the UV with an onset below 400 nm. Peak maxima in this region are found in solid state for **1** at ~263 nm (solution 247 nm) and **2** at ~250 nm (solution 242 nm). The latter can be attributed to $\pi-\pi^*$ transitions of the $PhSe^-$ and P^nPr_3 ligands. The weakly resolved absorption shoulders around ~290 (**1**) and 280 nm (**2**) in crystals of **1** and **2** are probably contributed by 4p → 5d ligand-to-metal charge-transfer transitions. Its onset is slightly shifted to the higher energies in the smaller cluster **2**. A dependence of the excitation energy versus size has been well documented for related pure cadmium selenide cluster compounds.[3,4] In addition to the strong UV features measured in dilute nujol mulls and solutions, **1** and **2** show weak absorption patterns between ~450 and ~600 nm in concentrated mulls and solutions. In difference to **1**, this pattern is well resolved in the solid-state spectrum of **2**, including peaks at 437, 465, and 495 nm and a shoulder at ~550 nm (Figure 5). Regarding the low extinction coefficients (~100 $M^{-1}cm^{-1}$) as well as PL data (see below), these absorption bands are assigned to spin-forbidden but symmetry-allowed d−d

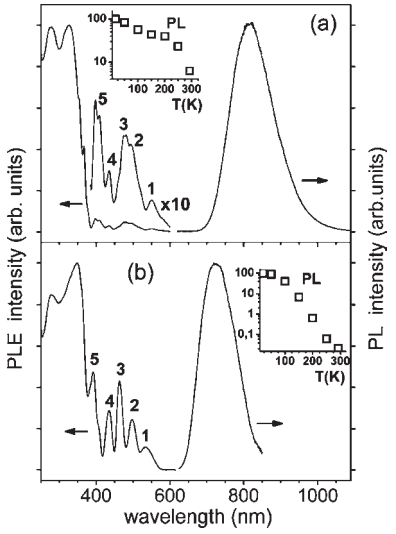

Figure 6. Photoluminescence excitation (PLE) and emission (PL) spectra (left and right panels, respectively) of (a) **1** and (b) **2** as mulls in nujol cooled down to 20 K. The PL spectra were taken at an excitation wavelength of 300 nm. PLE spectra were recorded at the emission peak wavelength. The PLE bands 1−5 are assigned to d−d optical transitions of the manganese(II) ions ($^4T_1(G)$, $^4T_2(G)$, [$^4E(G)$, $^4A_1(G)$], $^4T_2(D)$, $^4E_2(D) \leftarrow {}^6A_1$). The insets show the dependence of the integrated PL signal (emission band area) versus temperature.

transitions in the tetrahedrally coordinated manganese(II) ions.[41]

In the solid state and at temperatures below ~100 K, **1** and **2** show a bright red photoluminescence (PL) with a maximum at 780 and 725 nm (T = 20 K), respectively (Figure 6). By comparison with other compounds measured on the same apparatus, we roughly estimate the PL quantum yield of **1** and **2** to be no less than several percent. By increasing the temperature up to 293 K, the PL intensity of **2** decreases dramatically by a factor of 4500, whereas the PL of **1** only decreases by a factor of 15 and is readily visible under ambient conditions. Both complexes demonstrate nonexponential PL decay with a long-lived (major) component having a lifetime $\tau \sim 0.1$ ms at T = 20 K (when fit with a double-exponential decay). By increasing the temperature, the PL decays faster, correlating with the decrease of the PL intensity (Figure 6 insets). These results indicate that the PL decrease is due to thermally activated nonradiative relaxation channels, which are particularly effective in **2**.

In comparison to the absorption (Figure 5) and PL excitation (PLE) spectra of **1** and **2** measured at 293 K, their low-temperature PLE counterparts show well-resolved d−d absorption bands of manganese(II) (Figure 6). Five features numbered 1−5 are observed at 535, 497, 464, 435, and 392 nm for **2** and assigned to $^4T_1(G)$, $^4T_2(G)$, [$^4E(G)$, $^4A_1(G)$], $^4T_2(D)$, $^4E_2(D) \leftarrow {}^6A_1$ transitions, respectively.[41] The corresponding features for **1** are found at 550, 496, 478, 435, and ~404 nm.

The broad red PL with a large Stokes shift (Figure 6) is in contrast to a characteristic emission of inorganic manganese(II) compounds and manganese(II)-doped nanocrystals (e.g., 12-16 semiconductor quantum dots),[10] which has typically been observed in the green-to-orange

(41) Lever, A. B. P. *Inorganic Electronic Spectroscopy*, 2nd ed.; Elsevier: Amsterdam, The Netherlands, 1984, p 448.

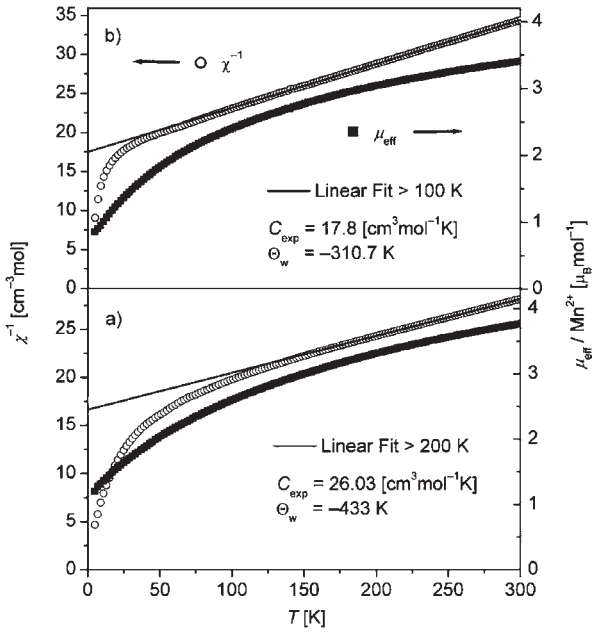

Figure 7. Plots of χ^{-1} (open circle, ○) and μ_{eff} (filled square, ■) versus temperature measured at 100 Oe for (a) $[Cd_4Mn_6Se_4(SePh)_{12}(P^nPr_3)_4]$ (**1**) and (b) $[Cd_4Mn_4S(SePh)_{14}(P^nPr_3)_2]$ (**2**). The straight line represents the best fit according to the Curie−Weiss law.

spectral region (depending on the manganese(II) surrounding) and attributed to $^6A_1 \leftarrow {}^4T_1(G)$ transition in manganese(II) ions. We tentatively assign the PL emission in **1** and **2** to delocalized excited state(s) contributed by the manganese(II) ions, Se(S) bridges, and P^nPr_3 ligands. A similarly red-shifted PL has been observed for manganese−benzimidazole complexes and attributed to metal-to-ligand charge-transfer (MLCT) states.[42]

Magnetic Properties. The magnetic susceptibility of **1** and **2** was measured in a field of 100 Oe (Figure 7). The curve of μ_{eff}/Mn(II) versus T for **1** shows a steady decrease by decreasing the temperature and does not reach a saturation value at high temperatures. This is in agreement with the large negative Weiss constant (−433 K) derived from a fit of the χ^{-1} versus T plot above 200 K. This indicates strong antiferromagnetic interactions which are consistent with our recent findings on the magnetism of selenolate-bridged manganese(II) compounds[15,43] and a related work on $[Mn_6Ge_4Se_{17}]^{6-}$.[44] The obtained Curie constant (26.0 cm^3 mol^{-1}K) is slightly smaller than that calculated for the presence of $6 \cdot S = 5/2$ Mn(II) (C = 26.3 cm^3 mol^{-1}K). A similar behavior is observed for **2**. Its Weiss constant (−310.7 K) is smaller indicating still strong but weaker antiferromagnetic coupling than found for **1**, while the Curie constant (17.8 cm^3 mol^{-1}K) derived from a linear fit of the χ^{-1} data above 100 K is only slightly larger than the calculated one ($4 \cdot S = 5/2$ Mn(II); C = 17.5 cm^3 mol^{-1}K). However the low-temperature behavior of **2** differs significantly from the temperature dependence of the suceptibility of isostructural $[Mn_4Se(SnSe_4)_4]^{10-}$,[45] which comprises a similar but selenium-bridged central Mn_4Se unit. The magnetic susceptibility of $[Mn_4Se(SnSe_4)_4]^{10-}$ shows a maximum at 17K before decreasing at lower temperatures, while for **2** it steadily increases from 300 to 5 K. Analyzing the magnetic data of **2** by using a fitting procedure to the appropriate Heisenberg spin Hamiltonian (see Experimental Section) only succeeded under additional consideration of a significant amount of paramagnetic impurities (PI). Given the similarity of the sulfur bridges between the four Mn(II) ions, we simplified the model by considering all six magnetic exchange interactions J between the metal atoms to be equal. The best set of parameters that fitted the experimental magnetic data was $g = 1.998$, $J = -9.25$ cm^{-1}, and PI = 8.6% (Figure S4, in the Supporting Information). The value of J is only slightly larger than found in structurally related $[Mn_4Se(SnSe_4)_4]^{10-}$ (J = 8.41 cm^{-1}). If we assume the crystalline sample to be almost pure (proven by X-ray powder diffraction, XRD, and elemental analysis), then the paramagnetic impurities could only originate from either the structural isomers of the ideal cluster composition $[Cd_4Mn_4S(SePh)_{14}(P^nPr_3)_2]$ or a distribution of cocrystallizing species with the general formula $[Cd_{4+x}Mn_{4-x}S(SePh)_{14}(P^nPr_3)_2]$ ($x < 0$ Mn enrichment; $x > 0$ Cd enrichment). Especially samples with $x > 0$ and/or an odd number of manganese atoms are likely to give rise to a paramagnetic (isolated Mn(II)) or ferrimagnetic behavior. These findings fit into the observations made by the other methods that the crystals of **1** and **2** should contain a certain distribution of isomers.

The coupling constants can also be estimated from the quantumchemically calculated data. From Figure 3 it is evident, that the energy difference of the low-spin broken symmetry state and the high-spin state of the most probable distribution is ca. 10 kJ/mol. For the low-spin state, one has four contacts of spin-up and spin-down manganese centers (none for the high-spin state), which are responsible for the energy lowering. The energy lowering per antiferromagnetic contact thus is ΔE = 2.5 kJ/mol, which by using the formula presented by Ruiz:[46]

$$J_{12} = \frac{\Delta E}{2S_1S_2 + S_1}$$

leads to $J \approx 14$ cm^{-1} ($S_1 = S_2 = 5/2$). This is reasonably close to the experimentally determined value of 9.2 cm^{-1}, as DFT (also B3-LYP) tends to overestimate magnetic coupling constants. Isothermal magnetization curves at 5 K (not shown) do not reach saturation up to 5 T for **1** and **2**.

Thermal Properties. Thermogravimetric analysis (TGA) of **1** in vacuum shows that the thermal decomposition occurs from 150 up to 350 °C in two successive steps (Figure 8). The mass change of the first reaction corresponds to the calculated cleavage of four P^nPr_3 (17.6%), while the mass loss in the second step is equivalent to six $SePh_2$ (calcd 38.4%). These results are similar to investigations on the related pure cadmium cluster $[Cd_{10}Se_4(SePh)_{12}(P^nPr_3)_4]$.[47] The solid residue of the

(42) Wei, Y.; Yu, Y.; Wu, K. *Cryst. Growth Des.* **2008**, *8*, 2087–2089.
(43) Eichhöfer, A.; Wood, P. T.; Viswanath, R. N.; Mole, R. A. *Eur. Inorg. Chem.* **2007**, 4794–4799.
(44) Melullis, M.; Clérac, R.; Dehnen, S. *Chem. Commun.* **2005**, 6008–6010.
(45) Brandmayer, M. K.; Clérac, R.; Weigend, F.; Dehnen, S. *Chem.—Eur. J.* **2004**, *10*, 5147–5157.
(46) Ruiz, E.; Rodriguez-Fortea, A.; Cano, J.; Alvarez, S.; Alemany, P. *J. Comput. Chem.* **2002**, *24*, 982–989.
(47) Eichhöfer, A. *Eur. J. Inorg. Chem.* **2005**, 1245–1253.

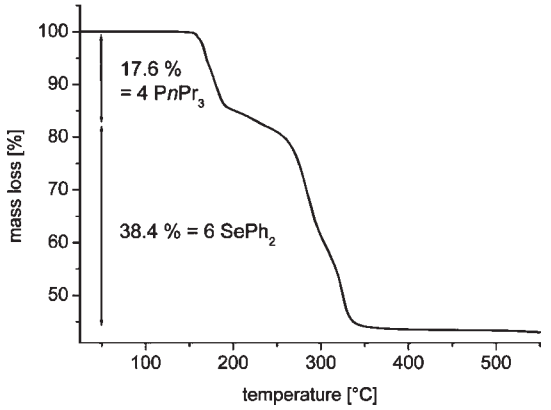

Figure 8. Thermogravimetric analysis of $[Cd_4Mn_6Se_4(SePh)_{12}(P^nPr_3)_4]$ (**1**) under vacuum (3×10^{-6} mbar). Heating rate is 2 K/min.

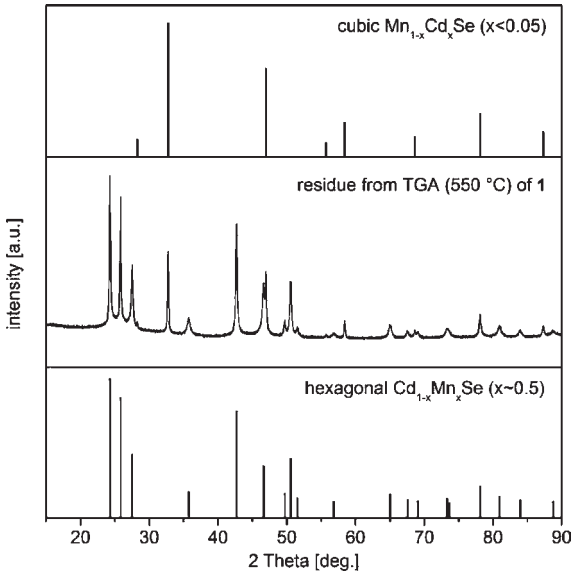

Figure 9. Powder XRD pattern of the residue of the TGA experiments under vacuum (3×10^{-6} mbar, up to 550 °C) of $[Cd_4Mn_6Se_4(SePh)_{12}(P^nPr_3)_4]$ (**1**) compared to the indexed reflection patterns of cubic $Mn_{1-x}Cd_xSe$ ($x < 0.05$) and hexagonal $Cd_{1-x}Mn_xSe$ ($x \approx 0.5$) (Table 2 and Tables S1 and S2, Supporting Information).

TGA of **1** heated up to 550 °C has the formal composition $Cd_{4.6}Mn_{5.4}Se_{10}$ and consists of two phases. The XRD powder pattern (Figure 9) reveals that in agreement with the phase diagram of the MnSe−CdSe system[48] the powder consists of a cubic $Mn_{1-x}Cd_xSe$ ($x < 0.05\%$) and a hexagonal $Cd_{1-x}Mn_xSe$ ($x \approx 0.5\%$) phase (Table 2 and Tables S1 and S2, Supporting Information).

Conclusion

We have described a successful and effective synthesis of two mixed Cd/Mn chalcogenide clusters $[Cd_4Mn_6Se_4(SePh)_{12}(P^nPr_3)_4]$ and $[Cd_4Mn_4S(SePh)_{14}(P^nPr_3)_2]$ by using bis-trimethylsilylamide transition-metal complexes soluble in organic solvents. Single crystal X-ray analyses and magnetic measurements supported by density functional theory (DFT) calculations suggest a kinetically controlled slight ion exchange on the metal atom positions in the solid state. First reactions with different stoichiometric ratios of the metal precursor complexes suggest that it is possible to adjust the overall cluster composition (narrow spectrum of different individuals) in a broad range for the same cluster cage. We, therefore, aim to investigate the possibility of a magnetic doping of for example $[Cd_{10}Se_4(SePh)_{12}(P^nPr_3)_4]$ cluster molecules with manganese(II) or other 3d metal ions.

Table 2. Lattice Constants of Hexagonal-CdSe and Cubic-MnSe Compared with the Cell Parameters Determined for the Two Indexed Phases[a]

	a [Å]	c [Å]	V [Å]^3
hex-CdSe[57]	4.299	7.010	112.2
hex-$Cd_{1-x}Mn_xSe$	4.234	6.892	107.0
cub-MnSe[58]	5.462		162.9
cub-$Mn_{1-x}Cd_xSe$	5.468		163.4

[a] Hex-$Cd_{1-x}Mn_xSe$ ($x \approx 0.5$) and cub-$Mn_{1-x}Cd_xSe$ ($x < 0.05$) formed in the TGA (550 °C) of $[Cd_4Mn_6Se_4(SePh)_{12}(P^nPr_3)_4]$ (**1**).

Experimental Section

Synthesis. Standard Schlenk techniques were employed throughout the syntheses using a double manifold vacuum line (10^{-3} mbar) with high-purity nitrogen (> 99.9999%). The solvent dme (dimethoxyethane) was dried over sodium-benzophenone and distilled under nitrogen. $Cd(N(SiMe_3)_2)_2$,[49] $Mn(N(SiMe_3)_2)_2$,[50] PhSeH,[51] and $Se(SiMe_3)_2$[52] were prepared according to literature procedures.

$[Cd_4Mn_6Se_4(SePh)_{12}(P^nPr_3)_4]$ (1). To a solution of $Cd(N(SiMe_3)_2)_2$ (0.23 mL (0.55 mmol)) in 30 mL of dme, P^nPr_3 (0.74 mL, 3.69 mmol) was added, and then HSePh (0.39 mL, 3.69 mmol) was added at 0 °C to give a colorless solution. Upon addition of $Mn(N(SiMe_3)_2)_2$ (0.54 mL (1.29 mmol)) the color of the solution turned red, followed after 30 min by addition of $Se(SiMe_3)_2$ (0.17 mL (0.74 mmol)). After one night in the refrigerator (2 °C), red cubic crystals of **1** started to form. They were filtered and washed with dme after completion of the crystallization after four days to give a total yield of 92% (0.46 g) with respect to Cd and 59.2% with respect to Mn. $C_{108}H_{144}Cd_4Mn_6P_4Se_{16}$ (3608.85): calcd C, 35.9; H, 4.0; Cd, 12.5; M_n, 9.1; found C, 35.7; H, 3.8; Cd, 12.5; M_n, 9.2.

$[Cd_4Mn_4S(SePh)_{14}(P^nPr_3)_2]$ (2). To a solution of P^nPr_3 (0.15 mL, 0.74 mmol) and HSePh (0.17 mL, 1.56 mmol) in 15 mL of dme, $Cd(N(SiMe_3)_2)_2$ (0.14 mL (0.35 mmol)) and $Mn(N(SiMe_3)_2)_2$ (0.16 mL (0.386 mmol)) were added to form a red solution immediately after the addition of $Mn(N(SiMe_3)_2)_2$. The following addition of $S(SiMe_3)_2$ (0.024 mL (0.12 mmol)) at 0 °C resulted in an orange-red color of the solution. After one night rhombic orange-red crystals of **2** started to form, which were filtered and washed with dme after five days to give a total yield of 225 mg (72.6% with respect to Mn and 80.1% with respect to Cd). Addition of the stoichiometric amount of $S(SiMe_3)_2$ (0.092 mmol) resulted in lower yields (40%) during the same reaction time. $C_{102}H_{112}Cd_4Mn_4P_2SSe_{14}$ (3206.85): calcd C, 38.2; H, 3.5; S, 1.0; M_n, 6.8; Cd, 14.0; found C, 38.2; H, 3.4; S, 0.9; M_n, 6.9; Cd, 13.8%

Crystallography. Crystals suitable for single crystal X-ray diffraction were taken directly from the reaction solution of the compound and then selected in perfluoroalkylether oil. Single crystal X-ray diffraction data were collected using graphite-monochromatized Mo Kα radiation ($\lambda = 0.71073$ Å) on a STOE IPDS II (imaging plate diffraction system). The structures were solved with the direct methods program SHELXS of

(48) Wiedemeier, H.; Sigai, G. *J. Solid State Chem.* **1970**, *2*, 404–409.
(49) Bürger, H.; Sawodny, W.; Wannagat, U. *J. Organomet. Chem.* **1965**, *3*, 113–120.
(50) Bürger, H.; Wannagat, U. *Monatsh. Chem.* **1964**, *95*, 1099–1102.
(51) Miyoshi, N.; Ishii, H.; Kondo, K.; Mui, S.; Sonoda, N. *Synthesis* **1979**, 301–304.
(52) Schmidt, H.; Ruf, H. *Z. Anorg. Allg. Chem.* **1963**, *321*, 270–273.

the SHELXTL PC suite programs[53] and were refined with the use of the full-matrix least-squares program SHELXL. Molecular diagrams were prepared using SCHAKAL 97.[54]

All Cd, Mn, Se, P and C atoms in **1** and **2** were refined with anisotropic displacement parameters, while hydrogen (H) atoms were calculated in fixed positions. In **1**, the positions of the cadmium and manganese atoms were refined with a mixed occupation (10% Mn on Cd(1) and Cd(2) and 10% Cd on Mn(1) and Mn(2). The *n*-propyl group C7−C9 of the phosphine ligand (P1) seems to be disordered (high Ueq of C8), however, an appropriate model could not be found. In **2**, the positions of manganese and cadmium atoms were also refined with mixed occupation (Cd(3) 0.8Cd/0.2Mn, Cd(4) 0.8Cd/0.2Mn, Mn(1) 0.9Mn/0.1Cd, Mn(2) 0.9Mn/0.1Cd, Mn(3) 0.9Mn/0.1Cd, and Mn(4) 0.9Mn/0.1Cd). Additional electron density close to Se13 was refined as one-tenth of a disordered Se15 atom. A corresponding disordered phenyl ring could not be located.

CCDC-762983(**1**) and 762984(**2**) contain the supplementary crystallographic data for this paper. These data can be obtained free of charge at www.ccdc.cam.ac.uk/conts/retrieving.html (Cambridge Crystallographic Data Centre, 12 Union Road, Cambridge CB2 1EZ, UK; fax: +44−1223/336−033; or e-mail: deposit@ccdc.cam.ac.uk).

X-ray powder diffraction patterns (XRD) were measured on a STOE STADI P diffractometer (Cu−Kα1 radiation, Germanium monochromator, Debye−Scherrer geometry) in sealed glass capillaries. Theoretical powder diffraction patterns for **1** and **2** were calculated on the basis of the atom coordinates obtained from single crystal X-ray analysis by using the program package STOE WinXPOW.[55]

Physical Measurements. Mass spectra were taken on a 7 T Fourier transform ion cyclotron resonance (FT-ICR) mass spectrometer (APEX II, Bruker Daltonics, Billerica MA, USA) equipped with an electrospray ionization (ESI) source (Analytica of Branford).

Methods of DFT using the program system TURBOMOLE[35] were applied to compound **2** with all phenyl and *n*-propyl groups exchanged by $-CH_3$. For several Cd/Mn distributions, the structure parameters of the high-spin state as well as of the low-spin broken-symmetry states were carried out using the BP86-functional[36,37] and def2-SV(P)[38] basis sets. Subsequently the energies were recalculated without further structure optimization using the B3-LYP functional[39] and larger def2-TZVP basis sets.[38]

UV−vis absorption spectra of cluster molecules in thf were measured on a Varian Cary 500 spectrophotometer in quartz cuvettes. For the preparation of concentrated solutions of **2**, 4 equiv of dimethylformamide (DMF) per cluster molecule were added. Solid-state spectra were measured in transmission as micrometer-sized crystalline powders between quartz plates with a Labsphere integrating sphere.

Photoluminescence measurements were performed on a Spex Fluorolog-3 spectrometer equipped with a closed-cycle optical cryostat operating at ∼20−293 K. R9910 and R5509 Hamamatsu photomultipliers (PMT) were used as photodetectors sensitive up to ∼850 and ∼1400 nm, respectively. Sample crystalline powders were placed as mulls in nujol between 1 mm thick quartz plates and mounted on a coldfinger of the cryostat. All emission spectra were corrected for the wavelength-dependent response of the spectrometer and detector (in relative photon flux units). Emission decay traces were recorded by connecting a PMT to an oscilloscope and using a N_2 laser for pulsed excitation (337 nm, ∼2 ns, ∼5 μJ).

Zero-field cooled temperature-dependent susceptibilities were recorded for **1** and **2** in RSO mode using a MPMS-5S (Quantum Design) SQUID magnetometer over a temperature range of 5−300 K in a homogeneous 100 Oe external magnetic field. The samples were contained in gelatin capsule filled in a glovebox under argon atmosphere, owing to the high degree of moisture and oxygen sensitivity of the compounds. The data were corrected for the sample holder and for diamagnetism using Pascal's constants.[56] Simulation of the experimental magnetic data with a full-matrix diagonalization of exchange coupling and Zeeman splitting was performed with the julX program (E. Bill, Max-Planck-Institut für Bioanorganische Chemie, Mühlheim an der Ruhr, Germany) using a spin Hamiltonian in the form:

$$\hat{H} = -2J \sum_{i=1,j>i}^{4} \vec{S}_i \vec{S}_j + \sum_{i=1}^{4} g_i \mu_B \vec{S}_i \vec{B}$$

Curie behaved paramagnetic impurities (PI) with $S = 5/2$ were included according to $\chi = (1 - \mathrm{PI}) \cdot \chi_{\mathrm{tetramer}} + \mathrm{PI} \cdot \chi_{\mathrm{mono}}$.

Thermogravimetric analyses were run in Al_2O_3 crucibles on a thermobalance STA 409 from Netzsch in vacuum (7×10^{-6} mbar) at a heating rate of 2 °C/min. The crucibles were filled (20−35 mg) inside an argon glovebox, transferred in Schlenk tubes and mounted under a stream of argon to the balance.

Acknowledgment. The authors are grateful to E. Tröster for her assistance in the practical work.

Supporting Information Available: Tables S1−S2, crystallographic data for the TGA products; Figures S1−S4, measured and simulated X-ray powder patterns for **1** and **2**, FT-ICR mass spectrum of **1**, UV−vis spectra of **1** and **2** in thf, and simulation of the magnetic data of **2**. Table S3, Cartesian coordinates, and total energies as a result of the DFT calculations for all treated compounds. This material is available free of charge via the Internet at http://pubs.acs.org

(53) Sheldrick, G. M. *SHELXTL PC*, version 5.1; Bruker Analytical X-ray Systems: Karlsruhe, Germany, 2000.
(54) Keller, E. *SCHAKAL 97*; Universität Freiburg: Freiburg, Germany, 1997.
(55) *STOE, WinXPOW*; STOE & Cie GmbH: Darmstadt, Germany, 2000.
(56) Kahn, O. *Molecular Magnetism*; Wiley-VCH: Weinheim, Germany, 1993.
(57) *Natl. Bur. Stand. Circ.* (*U. S.*) **1957**, *539*(7), 12.
(58) *Natl. Bur. Stand. Circ.* (*U. S.*) **1960**, *539*(10), 41.